

PHOTOPRODUCTION OF HADRONS AT HERA*

JAROSLAV CVACH

*Institute of Physics, Academy of Sciences of the Czech Republic, Na Slovance 2
Praha, CZ - 180 40, Czech Republic
E-mail: cvach@fzu.cz*

On behalf of the H1 and ZEUS collaborations.

ABSTRACT

New experimental results from photoproduction of hadrons at HERA are reviewed.

1. Introduction

The photoproduction of hadrons was in the first years of HERA experimentation the process to be studied most easily because of the large cross section. The recent results tend to investigate the domain of harder physics which can be compared with QCD calculations. In this contribution the latest results are reviewed which were presented¹ on the spring conferences of 1997 and are not covered by more specialized talks of this workshop. Specifically, I shall talk about inclusive particle production, resonances in multi-photon final state and prompt photons.

2. Inclusive particle production

The inclusive production of single hadrons in fixed target experiments and colliding beam experiments has been one of the important testing grounds for the QCD parton model. The HERA collider makes possible such studies in ep interactions over a wide range of squared four-momentum transfer, $-Q^2$, from photoproduction $Q^2 \approx 0$ to very high photon virtuality. Recent progress in the determination of parton fragmentation functions enables us to make specific predictions for inclusive particle production in next-to-leading order QCD. The parton distributions of the photon and the proton constitute an important input to the cross section calculations.

*To appear in the *Proceedings of the Ringberg Workshop: New Trends in HERA Physics*, Ringberg Castle, Germany, 25-30 May 1997.

2.1. Neutral strange particles

New results for K^0 and Λ inclusive photoproduction were obtained in the H1 experiment² for an average γp cms energy W of 187 GeV. K_S^0 mesons and Λ baryons are identified through their decay channels $K_S^0 \rightarrow \pi^+\pi^-$, $\Lambda(\bar{\Lambda}) \rightarrow p\pi^-(\bar{p}\pi^+)$, where the pion, the proton and the antiproton are reconstructed in the central jet chamber (CJC). In order to ensure an optimal acceptance of the CJC for neutral strange particles, their pseudorapidity has been restricted to $|\eta| < 1.3$ and their transverse momentum to $0.5 < p_t < 5$ GeV for K_S^0 and to $0.6 < p_t < 5$ GeV for Λ . All K_S^0

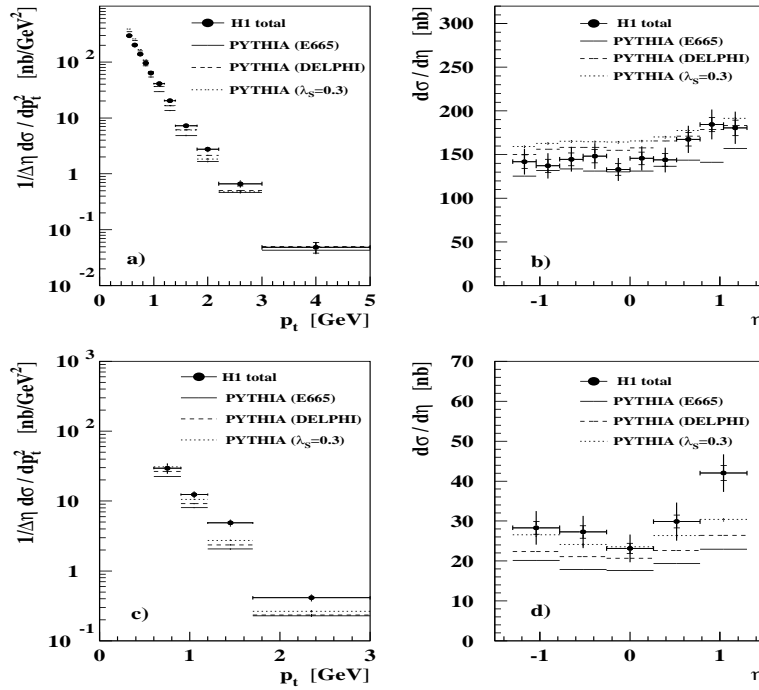


Fig. 1. Measured K^0 (a,b) and Λ (c,d) total ep cross section in photoproduction as a function of p_t and pseudorapidity η compared to PYTHIA in the kinematic range $|\eta| < 1.3$ and $0.5 < p_t < 5$ GeV.

results are multiplied by 2 and therefore correspond to $K^0 + \bar{K}^0$ production and are denoted by K^0 . As the Λ cross section is within errors equal to $\bar{\Lambda}$ cross section they are combined and referenced as Λ . Fig. 1 shows a comparison of the measured K^0 and Λ cross sections in p_t and η with the predictions of PYTHIA in combination with JETSET using standard parameter settings ($\lambda_s = 0.3$ as well as parameter sets obtained from fits to DELPHI and E665 data)^a. In the case of K^0 mesons the measured

^aThe following JETSET hadronization parameters have been changed with respect to the default

cross sections are in reasonable agreement with the Monte Carlo prediction using the DELPHI or E665 settings. However the measured Λ cross section lies significantly above the Monte Carlo prediction for all three settings. The UA5 collaboration has reported³ a similar discrepancy between Λ production in $\bar{p}p$ interactions at 200 GeV and PYTHIA predictions.

Recent NLO QCD calculations of inclusive spectra in ep scattering use fragmentation functions⁴ which have been fitted to e^+e^- data. A comparison of this calculation to data in the region of $p_t > 1.8$ GeV is satisfactory^{2,5}. If fragmentation is process independent, the rate of low p_t particles in γp and deep inelastic scattering (DIS) interactions will be the same. A comparison of K^0 production rates in γp and DIS⁶ is

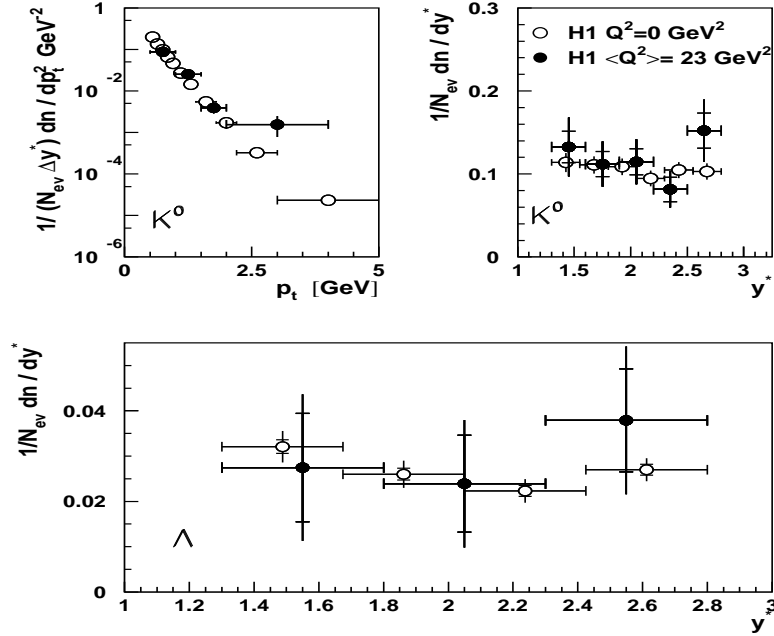


Fig. 2. K^0 rate as a function of p_t and centre of mass rapidity y^* (upper part) and Λ rate as a function of y^* (lower part) for non-diffractive events. γp data are represented by open and DIS data by closed circles. The inner vertical error bars indicate statistical error, the outer error bars the statistical and systematic error added in quadrature.

shown in Fig. 2 (upper part) and of Λ production rates in Fig. 2 (lower part) for the non-diffractive event samples^b. The γp and DIS rates are compatible in y^* and at low p_t (y^* is the γp cms rapidity defined with respect to the direction of the exchanged

settings (default/DELPHI/E665): $PARJ(2) = \lambda_s = (0.3/0.23/0.2)$, $PARJ(11) = 0.5/0.365/0.5$, $PARJ(12) = (0.6/0.41/0.6)$. $PARJ(2)$ is the strangeness suppression factor, $PARJ(11)$ ($PARJ(12)$) is the probability that a meson containing u or d (s) quark has spin 1.

^bFor non-diffractive samples H1 requires the presence of at least 500 MeV of energy in the forward region of the liquid argon calorimeter, $2.03 < \eta < 3.26$, to remove large rapidity gap events.

boson). Comparison between K^0 rates of production in $\bar{p}p$ collisions at 200 GeV obtained by the UA5 collaboration³ and this measurement show good agreement². In contrast, the Λ rates in the photon fragmentation region in photoproduction are significantly lower than in $\bar{p}p$ interactions. This may be attributed to the presence of an initial baryon in $\bar{p}p$ in this hemisphere from the incoming proton or antiproton. A difference between photon and target fragmentation region with respect to baryon production has also been observed in deep inelastic μN scattering⁷.

ZEUS examines⁸ the features of inclusive K^0 mesons produced with a high- E_t jet. The aim of the study is also to evaluate average longitudinal fragmentation function $D(z)$ for K^0 in jets from hard photoproduction and compare it with the fragmentation functions⁴ obtained in high energy quark jets in e^+e^- .

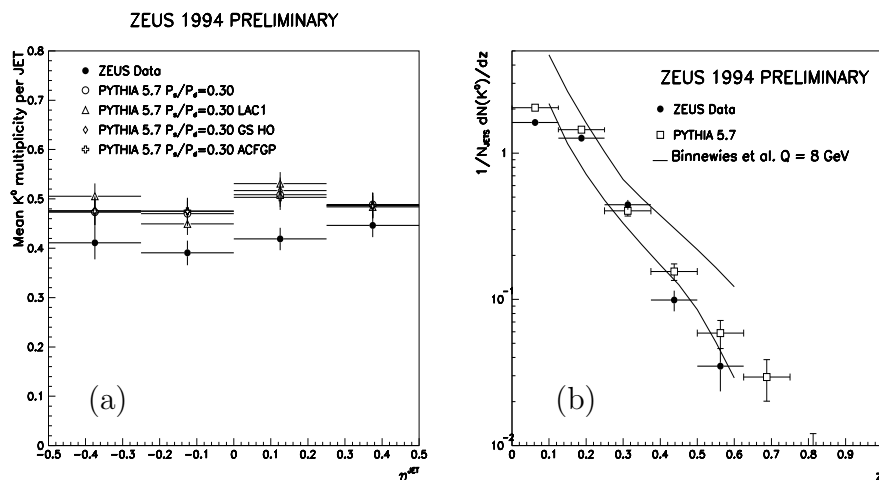


Fig. 3. (a) Corrected numbers of K_S^0 per jet as a function of jet pseudorapidity. (b) Corrected fragmentation function $D(z)$. Both distributions are defined with respect to 8 GeV hadron jets.

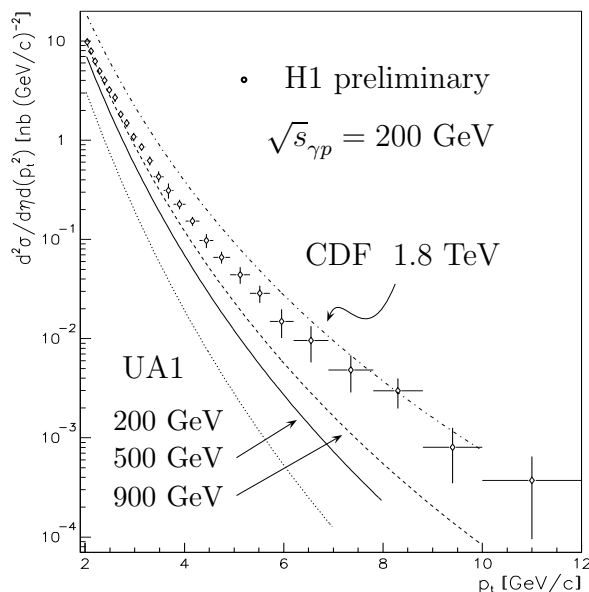
Events with at least one jet of $E_t > 8$ GeV and $|\eta^{jet}| < 0.5$ and K_S^0 with $0.5 < p_t < 4$ GeV and $|\eta| < 1.5$ were selected. The data were corrected to take into account effects due to reconstruction efficiency, event selection efficiency and bin-to-bin migration. Comparison of the mean number of K_S^0 per jet, integrated over $R \leq 1$ (R is the jet radius in cone algorithm in η and ϕ) are shown in Fig. 3a as a function of η^{jet} where the total number of jets was evaluated without the K_S^0 requirement. The shapes of the measured and Monte Carlo distributions are similar but the Monte Carlo is higher than data as observed also in other distributions. This discrepancy which cannot be explained by the size of systematic errors nor variation of MC parameters or photon parton densities is under investigation.

The distributions of particles within a jet may be described by the fragmentation function $D(z)$, where z is the longitudinal fraction of the jet momentum carried by the particle. Fig. 3b shows $D(z)$ for data compared to that from PYTHIA. Again K_S^0 distribution is lower than Monte Carlo by 20%. The curves are upper and lower

limits from the phenomenological fit of Binnewies et al.⁴ The lower curve corresponds to gluon fragmentation and the upper curve to s and u fragmentations and covers the spread of the fitted $D(z)$ values of fragmentation of u, d, s quarks using the LO and NLO schemes at a QCD scale of 8 GeV. The disagreement between data and phenomenological fit of $D(z)$ can be due to the fact that data are corrected to the hadron level to avoid the strong dependence of the correction to the parton level on the Monte Carlo used. One should keep in mind that e^+e^- data do not provide a sufficient constraint on $g \rightarrow K_S^0$ fragmentation and in this place the ep measurement is important.

2.2. Charged particles

Latest results of the inclusive transverse momentum spectra of charged particles in photoproduction events in the laboratory pseudorapidity range $-1.2 < \eta < 1.4$ have been measured up to $p_t = 8$ GeV using the ZEUS detector⁹ and in range $|\eta| \leq 1$ and $2 < p_t < 12$ GeV by H1¹⁰ at the average γp c.m. energy of $W = 200$ GeV. The inclusive transverse momentum spectra fall exponentially in the low p_t region. The non-diffractive data show a pronounced high p_t tail departing from the exponential shape. Comparison to hadron-hadron collisions¹¹ at a similar c.m. energy shows that the photoproduction data are clearly harder and in fact are similar to $\bar{p}p$ at $\sqrt{s} = 1.8$ TeV (see Fig. 4). In Fig. 5, the inclusive charged particle cross section $d\sigma/d\eta$



p_t spectrum is harder in γp due to:

- γp is measured in γ fragmentation region whereas $\bar{p}p$ in the central region
- γp behaves like Vp and parton momenta of quarks in the vector meson V are harder than in baryons
- dominance of direct part in γp cross section at high p_t can lead to harder scattering

Fig. 4. Inclusive cross section as a function of p_t for charged particles for $|\eta| < 1$. $\bar{p}p$ data were multiplied by 10^{-4} and fitted to the dependence $(1 + \frac{p_t}{p_{0,t}})^{-n}$. The text in the right part of the figure explains possible reasons of the difference between γp and $\bar{p}p$ distributions.

is shown for particles with $p_t > 2$ GeV. A comparison is made with PYTHIA with two different parton distribution functions: GRV-LO(Fig. 5a) and LAC1(Fig. 5b). None of the predictions match the data and they have mutually opposite slopes of the η distribution. From the figure it is clear that the rapidity distribution is sensitive to the photon structure function — the fact which will be pursued in the final analysis of the data with the aim to extract the gluon structure function of the photon. The inclusive

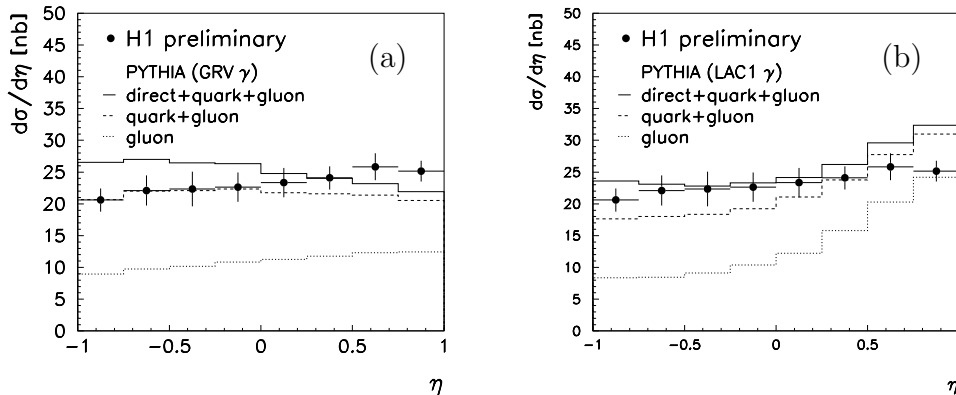


Fig. 5. Inclusive cross section as a function of η for charged particles with $p_t > 2$ GeV compared to PYTHIA with the GRV-LO(a) and LAC1(b) photon parton parametrizations.

distributions of charged particles were compared with NLO QCD calculations. Good agreement is observed in p_t distribution in the whole measured range of $p_t > 2$ GeV as well as in $d\sigma/d\eta$ distribution⁵.

3. Scale influence on the energy dependence of photon-proton cross section

The energy dependence of the real photon-proton total cross section is consistently described at high energies by the power law $\sigma_{\gamma p}^{tot} \propto (W^2)^\lambda$, where W is the γp centre of mass energy and the power $\lambda \sim 0.08$. In contrast, the virtual photon-proton cross section is found to rise faster^{12,13} with increasing W^2 for Q^2 values larger than a few GeV^2 . In the HERA regime fits of the form $\sigma_{\gamma^* p}^{tot} \propto (W^2)^\lambda$ lead to values of λ which rise^{13,12} from 0.2 to 0.4 in the Q^2 range from 1.5 to 10^3 GeV^2 (see Fig. 6). The change of the slope parameter λ with increasing Q^2 is associated with a transition from the non-perturbative ‘soft’ to the perturbative ‘hard’ regime¹⁴. The perturbative QCD (pQCD) can be applied in the domain where Q^2 is larger than a few GeV^2 and it predicts an increase of λ with Q^2 . In the Reggeon Field Theory (RFI) the change of λ can be interpreted as a reduction of screening corrections¹⁵ with increasing Q^2 . RFI and pQCD are two complementary approaches which successfully describe physics processes in different regimes - ‘soft’ and ‘hard’.

Whereas in DIS the hardness of the interaction (scale) can be characterized by the photon virtuality Q^2 , in photoproduction with $Q^2 \approx 0$ the largest p_t of a hadron in

the photon fragmentation region can take over the role of the scale. This investigation was the subject of the study discussed in this chapter the results of which have been published recently¹⁶.

In total about two million photoproduction events were selected in the energy range $150 < W_{\gamma p} < 250$ GeV. The W dependence of the cross section was measured in different bins of the maximal $p_{t,max}$ of the charged particle in an event. Good detector

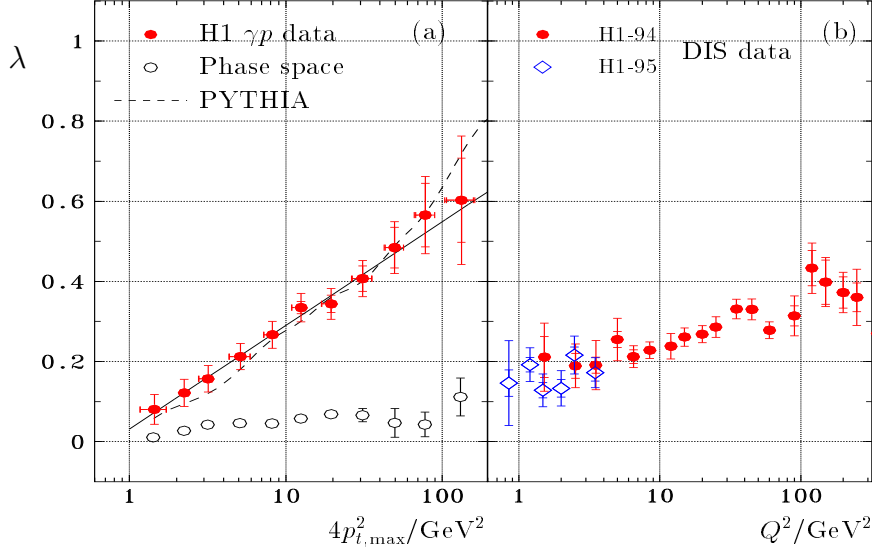


Fig. 6. Slope λ of the W^2 dependence of the photoproduction (a) and DIS (b) cross section as a function of $4p_{t,max}^2$ and Q^2 respectively.

acceptance and high resolution of p_t measurement together with large statistics of photoproduction events, allow a continuous coverage of both soft and hard domains in the pseudorapidity range $1.1 < \eta^* < 3.1$ (η^* is measured with respect to the γ direction in the γp centre of mass system). The energy dependence of the cross section in each $p_{t,max}$ bin was fitted to the form $\sigma(W, p_{t,max}^2) \sim W^{2\lambda(p_{t,max}^2)}$. The results of the fit are shown in Fig. 6, where the slope λ is given as function of $4p_{t,max}^2$. A strong increase of λ is observed with increasing $p_{t,max}$ which can be fitted by a straight line. Note that when the scale $4p_{t,max}^2$ is multiplied with a number, this does not change the slope of the straight line. Hence the change of λ with the scale is significant. Comparison with the longitudinal phase space model shows that the phase space plays only a minor role.

On the other hand the $p_{t,max}$ dependence of λ is described by PYTHIA. The model is based on the Monte Carlo version which includes both pQCD for the hard scattering and a Regge inspired soft interaction component. It was checked that the effects of different proton and photon structure function, of parton showers as well as multiple parton-parton scattering are small. Therefore, the change of the slope λ is not associated with the growth of the gluon density in the proton at small x but

rather with the leading order matrix element of the hard process in PYTHIA.

4. Resonances in multi-photon final state

As mentioned already in the previous chapter the energy dependence of soft photon-hadron interactions at high energies are well described¹⁷ by the Reggeon Field Theory provided that the exchange of Pomeron trajectory with the quantum numbers close to vacuum, i.e. with the intercept $\alpha(t=0) \approx 1.08$ and C parity $+1$ is introduced. No direct evidence has been found at high energies for an exchange of trajectory with the same intercept but with $C = -1$ called Odderon trajectory. At HERA the existence of an Odderon trajectory could result in the production of pseudoscalar mesons with $C = +1$ in addition to their production via the two photon fusion process. Schäfer et al.¹⁸ suggest to measure the cross section ratio for exclusive production of η 's and η' 's since the sensitivity to the Odderon contribution differs for η and η' . Assuming the coupling to the meson for photon-Odderon fusion being proportional to the product of the electric charge and the baryon number of the quarks composing the meson, η - being predominantly in the octet state with respect to flavour $SU(3)$ - gets larger contribution compared to η' being dominantly the singlet. The data were

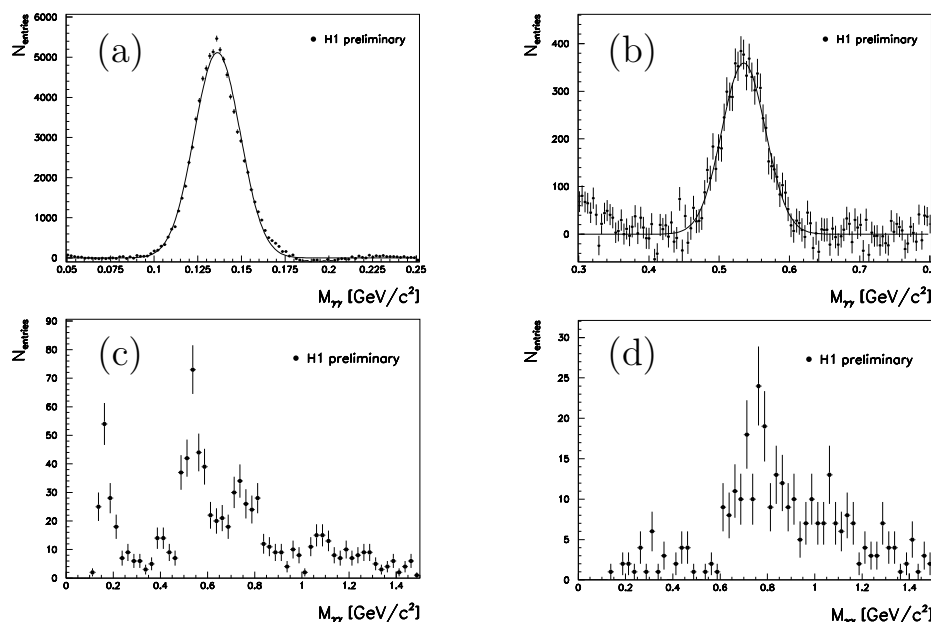


Fig. 7. Invariant mass spectra of 2γ 's: (a) π^0 mass region for photon energies $E_\gamma > 1$ GeV after background subtraction (b) η mass region for photon energies $E_\gamma > 1.5$ GeV after background subtraction (c) events with a vertex and $E_\gamma > 0.7$ GeV (d) events without a vertex and $E_\gamma > 0.7$ GeV.

taken in 1996 with the H1 detector and amount to an integrated luminosity of about 5 pb^{-1} . The lead/scintillating fibre calorimeter SPACAL¹⁹ has a sampling term of

$7\%/\sqrt{E/\text{GeV}}$ and a position resolution of about 5 mm at 1 GeV. Together with the threshold ≈ 100 MeV this allows for a precise measurement of mesons decaying into multi-photon final states, e.g. of π^0 and η mesons in their 2γ decay mode, as shown in Fig 7. The central values of the Gaussian fit amount to 136 MeV for π^0 and 535 MeV for η . The measured width of the invariant mass distribution is $\sigma \approx 13$ MeV for π^0 and $\sigma \approx 31$ MeV for η , demonstrating the good performance of the detector.

The acceptance of the positron calorimeter of the luminosity system restricts the photon energy in the laboratory system to lie between 8 and 20 GeV and to a photon virtuality $Q^2 < 0.01 \text{ GeV}^2$. The selected events consist of the scattered positron, two photons within the angular acceptance of the SPACAL ($-3.8 < \eta^\gamma < -1.4$, η^γ is photon laboratory rapidity), and an elastically scattered proton which escapes undetected in the main detector.

Selected events with a reconstructed vertex, i.e. with at least one charged track in the central detector, result in the invariant mass spectrum of photon pairs as shown in 7c. A clear signal of π^0 and η mesons are observed, no indication for a signal of the η' meson at the mass 958 MeV is found. By requiring no charged particles in the central detector (events without a reconstructed vertex) is compatible with exclusive meson production. It leads to the invariant mass spectrum of the photon pairs as shown in 7d. No signal of exclusively produced η and η' mesons is observed nor of π^0 . The resonance-like structure at an invariant mass of about 800 MeV is interpreted as being due to elastic photoproduction of ω mesons and their subsequent decays into the $\gamma\pi^0$ final state, where only two out of three photons are detected.

The non-observation of η mesons is compatible with the expectation from a pure two photon fusion process, given the small acceptance of the detector. This excludes a large contribution from Odderon induced process with cross section substantially larger than the two photon fusion cross section. In the case of η' the small branching ratio of 2.12% further reduces the expected number of events by an order of magnitude. The analysis continues to quantify the results into the cross section upper bounds for exclusive production of π^0 , η and η' mesons.

5. Observation of isolated high E_t photons at HERA.

The ZEUS detector identified a class of events showing the characteristics of high E_t isolated photons termed here as “prompt” to distinguish them from those produced via particle decays. This is the first observation of prompt photons at γp centre of mass energies an order of magnitude higher than those previously employed. In the kinematic range covered by HERA detectors, the prompt photons are produced predominantly in two hard subprocesses²⁰ which in LO are represented as the Compton scattering $\gamma q \rightarrow \gamma q$ in the direct channel and by $qg \rightarrow \gamma q$ in the resolved channel. NLO QCD adds additional processes where hard photon is radiated from outgoing quarks. Due to the electromagnetic nature of the photon the prompt photon pro-

duction is suppressed approximately by a factor α with respect to hard processes involving partons only which represent the main source of background. Therefore, a sophisticated data analysis must be done to isolate events with prompt photons from background. A particular virtue of prompt photon processes is that the observed final-state photon emerges from the QCD process directly, without the intermediate hadronisation of final state partons into jets.

The data correspond to an integrated luminosity of 6.36 pb^{-1} collected by the ZEUS detector in 1995 in e^+p collisions with energy $E_e = 27.5 \text{ GeV}$ with protons of energy $E_p = 820 \text{ GeV}$. Photons were detected in the barrel part of the uranium-scintillator calorimeter in its electromagnetic section (BEMC) which restricts the photon pseudorapidity range to $-0.75 < \eta^\gamma < 1.0$. A standard ZEUS electron finding algorithm was used to identify photon signal with $5 < E_t^\gamma < 10 \text{ GeV}$. A cone jet finding algorithm was used to identify jets with $E_t^{jet} > 5 \text{ GeV}$, pseudorapidity $-1.5 < \eta^{jet} < 1.7$ and unit cone radius, using entire ZEUS calorimeter system. Events with an observed DIS electron were removed, restricting incoming photon virtualities to $Q^2 \leq 1 \text{ GeV}^2$. Isolation cone criteria were applied on the photon candidate to reduce possible background from radiation of electrons or positrons and from energy fluctuation of jets into hard π^0 or η . Two shape-dependent quantities were studied in order to distinguish photon, π^0 and η signals. These were the energy weighted mean width of the BEMC cluster in z direction z_{width} and the energy fraction of the most energetic cell in the cluster F_{max} (Fig. 8a) of the photon candidate. The relative

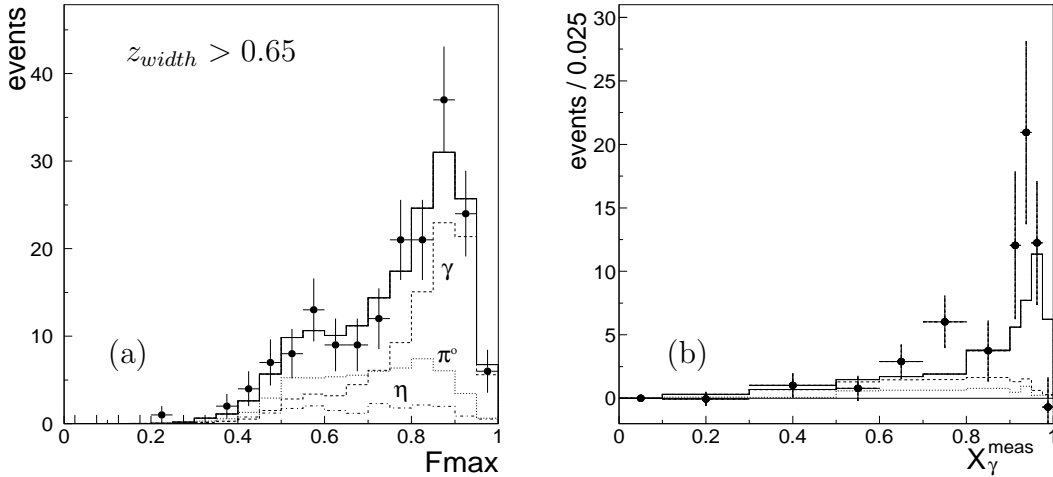


Fig. 8. (a) Distribution of F_{max} for prompt photon candidates and γ, π^0, η fitted Monte Carlo. z_{width} given in BEMC cell units (b) x_γ^{meas} of prompt photon after background subtraction. (•) data points, histogram - Monte Carlo: (···) quark radiation, (—) q rad+resolved, (—) q rad+resolved+direct.

amounts of γ, π^0 and η from single particle Monte Carlo distributions were obtained from fits of z_{width} and F_{max} to data. To get distribution of physical quantities, a background subtraction is applied on the assumption that the data may be expressed

as a sum of the photon signal plus neutral meson background. The result for the fraction x_γ of the incoming photon momentum that contributes to the production of the high E_t photon and jet $x_\gamma^{meas} = \sum_{jet+\gamma}(E-p_z)/\sum_{event}(E-p_z)$ is shown in Fig. 8b. The Monte Carlo distributions are normalised to the same integrated luminosity as data. A strong peak near $x_\gamma^{meas} = 1$ corresponds to the Compton process. It is not possible to make conclusions concerning the presence of a resolved photon component. The background distribution is consistent with zero for $x_\gamma^{meas} > 0.9$. The quoted cross section for the process $ep \rightarrow e + \gamma_{prompt} + jet + X$ with $x_\gamma^{meas} \geq 0.8$ is $15.3 \pm 3.8(\text{stat}) \pm 1.8(\text{syst})$ pb in the kinematic range defined above. The systematic error is dominated by 8% contribution due to the uncertainty in the calorimeter calibration. The cross section is in an agreement with the NLO QCD calculation²¹.

6. Conclusion

Inclusive particle production provides a complementary view on hard scattering to the commonly more used jet production. Selecting events with a hadron with p_t at least 1 – 2 GeV, the inclusive spectra are calculable in QCD and are sensitive to structure functions of beam projectiles — photon (real or virtual) and proton. It will be the task of the coming years of HERA hadron physics to use inclusive spectra of hard hadrons to obtain the gluon structure function of the real photon. Events with prompt photons have a sensitivity to the quark content of the photon. With the increase of HERA luminosity they will supplement the inclusive spectra of charged particles in the study of partonic structure of the photon.

7. Acknowledgement

It is a pleasure for me to thank my colleagues from ZEUS and H1 collaboration who helped to prepare this talk and provided me with results and figures. I would also like to thank the organizers of the workshop for a very friendly atmosphere and a place for many stimulating discussions during the workshop.

This work is supported by the Grant Agency of Academy of Sciences of the Czech Republic under the grant no. A1010619 and by the Grant Agency of the Czech Republic under the grant no. 202/96/0214.

8. References

1. Talks presented at the International Conference Photon-97, Egmond aan Zee, The Netherlands, May 1997:
D. Milstead, High p_t charged particles and strangeness photoproduction and comparison with DIS at HERA,
N. Gogitidze, Scale influence on the energy dependence of the photon-proton

- cross section and F_2 at low Q^2 ,
S. Tapprogge, Resonances in the multi-photon final states in positron-proton scattering at HERA,
T. Vaiculis, Observation of isolated high E_t photons in hard photoproduction at HERA.
2. H1 Collab., C. Adloff et al., DESY-97-095, to be published in *Z. Phys.* **C**.
 3. UA5 Collab., R.E. Ansorge et al., *Nucl. Phys* **B328** (1989) 36;
 ibid. *Z. Phys.* **C41** (1988) 179.
 4. J. Binnewies, B. A. Kniehl, G. Kramer, *Phys. Rev.* **D53** (1996) 3573.
 5. B. A. Kniehl, in the contribution to this Proceedings, hep-ph/9709261.
 6. H1 Collab., S. Aïd et al., *Nucl. Phys.* **B480** (1996) 3.
 7. E665 Collab., M. R. Adams et al., *Z. Phys.* **C61** (1994) 539.
 8. ZEUS Collab., paper submitted to ICHEP96 pa02-044.
 9. ZEUS Collab., M. Derrick et al., *Z. Phys.* **C67** (1995) 227.
 10. W. Hoprich, *Diplomarbeit*, I. Phys. Institut, Univ. Heidelberg, 1995;
 H1 Collab., paper 270 submitted to ICHEP97.
 11. CDF Collab., F. Abe et al., *Phys. Rev. Lett.* **61** (1988) 1819;
 UA1 Collab., C. Albajar et al., *Nucl. Phys.* **B335** (1990) 261.
 12. ZEUS Collab., M. Derrick et al., *Z. Phys.* **C69** (1996) 607.
 13. H1 Collab., C. Adloff et al., *Nucl. Phys.* **B497** (1997) 3.
 14. A. Levy, TAUP 2349-96, hep-ex/9608009.
 15. A. Capella, A. Kaidalov, C. Merino, J. Tran Than Van, *Phys. Lett.* **B337** (1994) 358.
 16. H1 Collab., S. Aïd et al., *Phys. Lett.* **B392** (1997) 234.
 17. A. Donnachie and P. V. Landshoff, *Phys. Lett.* **B296** (1992) 227.
 18. A. Schäfer, L. Mankiewicz and O. Nachtmann, Proceedings of *Future Physics at HERA*, eds. G. Ingelman, A. De Roeck, R. Klanner, DESY 1996, p. 243.
 19. H1 SPACAL group, R. D. Appuhn et al., *Nucl. Instrum. Methods* **A374** (1996) 149.
 20. P. Aurenche, P. Chiappetta, M. Fontannaz, J. P. Guillet, E. Pilon, *Z. Phys.* **C56** (1992) 589; L. E. Gordon and W. Vogelsang, *Phys. Rev.* **52D** (1995) 58.
 21. L. E. Gordon, talk presented at the International Conference Photon-97, Egmond aan Zee, The Netherlands, May 1997.